

Type of Contribution: Original Research Article

Influence of temperature on production of water-in-oil emulsions by microchannel emulsification

Katerina Butron Fujiu^{a,b}, Isao Kobayashi^{a,*}, Marcos A. Neves^{a,b}, Kunihiro Uemura^a and Mitsutoshi Nakajima^{a,b,*}

^a *Food Engineering Division, National Food Research Institute, NARO, 2-1-12 Kannondai, Tsukuba, Ibaraki 305-8642, Japan*

^b *Faculty of Life and Environmental Sciences, University of Tsukuba, 1-1-1 Tennoudai, Tsukuba, Ibaraki 305-8572, Japan*

* To whom correspondence should be addressed.

e-mails: isaok@affrc.go.jp (I. Kobayashi), nakajima.m.fu@u.tsukuba.ac.jp (M. Nakajima)

Running title: Temperature influence on microchannel W/O emulsification

Abstract

In this paper, we report the influence of temperature on the production characteristics of water-in-oil (W/O) emulsions by microchannel emulsification (MCE). The temperature of an emulsification module including a hydrophobic microchannel (MC) array chip was controlled between 10°C and 55°C. The continuous phase was a decane oil solution containing 5wt% tetraglycerin monolaurate condensed ricinoleic acid ester as a surfactant. The dispersed phase was a Milli-Q water solution containing 1wt% of sodium chloride and 5wt% of polyethylene glycol. The contact angle of the dispersed phase on the MC wall exceeded 152°, strongly suggesting that the MC array surfaces are not wetted by the dispersed phase during MC emulsification. At the breakthrough pressure of the dispersed phase, monodisperse W/O emulsions with coefficient of variation below 5% were produced via hydrophobic MC arrays, irrespective of the temperature. At each operating temperature, the resultant droplet diameter was also almost constant below a critical flow velocity of the dispersed phase. The maximum droplet generation rate from a channel gradually increased with increasing operating temperature due to the decrease in viscosity of both phases. An adapted capillary number that considers the influence of the wettability and surfactant adsorption had a low maximum/minimum value ratio of 1.2.

Keywords: Microchannel emulsification, Temperature, W/O emulsion, Contact angle, Viscosity.

1. Introduction

Water-in-oil (W/O) emulsions, which are usually stabilized by oil soluble surfactants, are dispersions with important applications in foods, medicines, pharmaceuticals, cosmetics, and chemicals. W/O emulsions are also commonly prepared as a dispersed phase for producing water-in-oil-in-water (W/O/W) emulsions [1-3]. Aqueous droplets dispersed in W/O emulsions are micro-compartments useful for encapsulating hydrophilic active substances [4]. The average droplet size and droplet-size distribution are the most important parameters determining many properties of emulsions with the same composition [5]. For instance, these parameters influence the stability (in terms of Ostward ripening, coalescence, and sedimentation), rheology, chemical reactivity, and physiological efficiency (e.g., the release properties of encapsulated active substances) of W/O emulsions [6]. Monodisperse emulsions with very narrow droplet-size distributions are highly desirable because they have better coalescence stability than polydisperse emulsions [7] and enable simplified interpretation and easier control of emulsion properties [8,5].

Temperature-controlled emulsification is required for producing emulsions containing high-melting-point or thermo-sensitive substances. A typical example of temperature-controlled emulsification is the production of W/O emulsions containing high-melting-point lipids as part of the margarine manufacturing process. This emulsification process is normally conducted at temperatures around 50°C to 60°C. Kukizaki et al. [9] produced W/O and W/O/W emulsions using a tripalmitin oil phase at an elevated temperature of 60°C. The resultant W/O/W emulsions encapsulating vitamin B₁₂ in the internal aqueous phase were immediately cooled to obtain dispersions containing solid lipid microcapsules. Low-temperature emulsification is also expected to suppress the degradation of heat-sensitive active substances (e.g., vitamins and biological molecules).

W/O emulsions are normally produced with traditional emulsification devices, such as rotor-stator systems (stirred vessels, colloid mills, or toothed-disk dispersing machines),

high-pressure homogenizers, and ultrasonic homogenizers. Such devices apply shear, extension, and impact to two-phase systems, disrupting large droplets into smaller ones [5]. They also generate a huge amount of heat during operation, resulting in considerable temperature elevation of the emulsion products. While most of these devices are equipped with thermo-control units, it is difficult to make the temperature in the entire device uniform. The resultant W/O emulsions are usually polydisperse with a typical coefficient of variation (CV) over 20%. The droplet size is controlled empirically.

Nakashima et al. [10] introduced membrane emulsification (ME) as a technique for producing monodisperse emulsions. ME produces emulsions by forcing a dispersed phase through membrane pores into a (cross-flowing) continuous-phase domain. This process enables low-energy input due to droplet generation at low mechanical stress, reducing temperature elevation [11]. Shirasu Porous Glass (SPG) membranes containing relatively uniform pores with non-circular cross-sections are most commonly used for ME [4,12]. SPG membranes with hydrophobically modified surfaces have been used for producing monodisperse W/O emulsions containing relatively uniform droplets with the smallest CV of about 10% [13,14]. To our knowledge, no ME study focusing on the quantitative effect of temperature has yet been reported.

Kawakatsu et al. [15] introduced microchannel emulsification (MCE), which is capable of producing monodisperse emulsions containing uniform droplets with the lowest CV (below 5%). MCE produces emulsions by a unique process called “spontaneous droplet generation” with no external shear force and very low energy input [16]. This droplet generation process driven by interfacial tension is advantageous when using shear and thermo-sensitive components (e.g., proteins and starches). Microchannel (MC) arrays fabricated for MCE use are classified into grooved MC arrays, each consisting of parallel MCs and a terrace [15], and straight-through MC arrays, each consisting of compactly arranged straight-through MCs [7]. A major advantage of grooved MC arrays is that one can clearly observe the movement of the

water-oil interface around them during droplet generation, while it is difficult to experimentally observe inside straight-through holes. By contrast, straight-through MC arrays have much higher droplet production rates than grooved MC arrays. For a given MC size, a straight-through MC array chip can accommodate over 100 times more MCs per unit area than a grooved MC array chip.

Silicon MC array chips are usually used for MCE. Hydrophobically surface-modified MC arrays have mostly been employed to produce monodisperse W/O emulsions[15-19]. Polymeric MC arrays, which are intrinsically hydrophobic, also produce monodisperse W/O emulsions [18,20]. In MCE, monodisperse W/O emulsions are successfully produced using appropriate hydrophobic surfactants that can prevent wetting of a dispersed phase onto the MC surface [17]. In addition, the osmotic pressure of the dispersed aqueous phase has to be high enough to suppress the migration of water molecules via the water-oil interface [19]. Alkane oils of low viscosity are generally used as the continuous-phase medium for MCE. Triglyceride oils can also be used as the continuous-phase medium [19].

MCE research on the production of W/O emulsions is normally carried out at an ambient temperature of 25°C. MCE at elevated temperatures has been performed for producing monodisperse gelatin microbeads [21]. Temperature influences the physical and physicochemical properties of the two phases, such as their viscosity and interfacial tension, as well as the solubility of the surfactant in the continuous phase. Thus, temperature is assumed to play an important role in producing W/O emulsions besides their stability. We recently investigated the influence of temperature on the production of O/W emulsions by MCE [22], but it is still unclear how temperature influences the production of W/O emulsions by MCE.

The objective of this study was to systematically investigate the influence of temperature on the production of W/O emulsions by MCE. We analyzed the MCE results for droplet size, droplet-size distribution, droplet productivity, and droplet generation at different temperatures

between 10°C and 55°C. The physical and physicochemical properties of the W/O system were also investigated at the temperatures applied to MCE.

2. Materials and Methods

2.1 Chemicals

Decane, purchased from Wako Pure Chemical Ind. (Osaka, Japan), was used as the medium for all of the continuous-phase solutions. Tetraglycerin monolaurate condensed ricinoleic acid ester (CR-310), provided by Sakamoto Yakuhin Kogyo Co., Ltd. (Osaka, Japan), was used as the oil-soluble surfactant. Milli-Q water was used to prepare the dispersed-phase solutions. NaCl, purchased from Wako Pure Chemical Ind., was used for suppressing migration of water molecules via the water-oil interface [19]. Polyethylene glycol (PEG, M.W.: 20,000), purchased from Wako Pure Chemical Ind., was used for increasing the dispersed-phase viscosity. A silane coupler reagent, octadecyltriethoxysilane (L-6970), was purchased from Shin-Etsu Chemical Co., Ltd. (Tokyo, Japan). All of the chemicals were used as received.

2.2 Emulsification setup

A schematic diagram of the experiment setup used for MCE is presented in Fig. 1a. The MCE setup consists of a temperature-controllable module equipped with an MC array chip (Model: CMS6-1), a 10-mL liquid chamber that contains a dispersed phase, a syringe pump (Model 11, Harvard Apparatus Inc., Holliston, USA) that feeds the continuous phase with a 50-mL glass syringe, and a microscope high-speed video system [22]. The temperature inside the module can be controlled using a water circulator equipped with heating and cooling units (EYELA Digital Uni Ace-100, Tokyo Rikakikai Co., Ltd., Tokyo, Japan).

Figure 1b is a schematic representation of a silicon MC array chip with dimensions of 25 x 28 x 0.5 mm. The MC array chip has 10 MC arrays, each consisting of 107 parallel channels with a depth of 5 μm , a width of 8 μm , and a length of 140 μm and a terrace with a depth of 5 μm and a length of 40 μm . Each continuous-phase channel outside the terrace outlet has a depth of 100 μm . The MC array chip as well as a glass plate used for producing W/O

emulsions had hydrophobic surfaces, having been treated with a silane couple reagent according to the method reported by Kobayashi et al. [19].

2.3 Preparation of solutions

The continuous phase was prepared by dissolving 5wt% CR-310 into decane. To improve the stability of the W/O emulsion droplets, the decane was pre-treated prior to use as follows. Decane was mixed with water using a magnetic stirrer at a volume ratio of 9:1 (decane:water) for 45 min. Following that, the phases were separated by centrifugation at 1500 x g for 20 min using a table centrifuge (KN-70, Kubota Co., Tokyo, Japan) [23]. The decane supernatant phase was used for preparing the continuous phase. The dispersed phase was prepared by dissolving 5wt% PEG and 1wt% NaCl into Milli-Q water.

2.4 Emulsification procedure

Droplet-generation experiments were performed with the MCE setup depicted in Fig. 1a. The MC array chip was rinsed with the continuous phase prior to each experiment and was then mounted into a module filled with the continuous phase during assembly. After adjusting the temperature of the assembled module, the pressurized dispersed phase was introduced into the module. The pressure applied to the dispersed phase (ΔP_d) was gradually increased. ΔP_d can be given by

$$\Delta P_d = \rho_d \Delta h_d g \quad (1)$$

where ρ_d is the dispersed-phase density, Δh_d is the difference in the hydraulic heads between the chamber containing the dispersed phase and the channels of the module, and g is the acceleration due to gravity. To generate droplets, the dispersed phase was forced through the MCs onto the terrace and into the continuous-phase channel (Fig. 1c). During MCE, droplet generation, regulated by tuning the chamber height, was monitored at a frame rate of 1000 fps using the microscope high-speed video system. The most upstream-side MCs, which were

close to the inlet hole for the dispersed phase, were considered in this study. MCE experiments were carried out at different temperatures (T_C) of 10, 25, 40, and 55°C. Three separate experimental runs were conducted at each temperature.

The hydrophobic MC array chip used for each MCE experiment was cleaned using an ultrasonic bath (VS100III, As One Co., Osaka, Japan) at a frequency of 45 kHz as follows. The MC array chip was cleaned in Milli-Q water for the first 20 min, in Milli-Q water containing ethanol (1:1 v/v proportion) and non-ionic detergent for the next 20 min, and in Milli-Q water for the final 20 min.

2.5 Measurement and analysis

The density of the liquid phases was measured with a density meter (DA-130 N, Kyoto Electronics Manufacturing Co., Ltd., Kyoto, Japan). Their viscosities were measured with a vibro viscometer (SV-10, A&D Co. Ltd., Tokyo, Japan). The equilibrium interfacial tension was measured by the pendant drop method (PD-W, Kyowa Interface Sciences Co., Ltd., Saitama, Japan). The contact angle of the interface with the MC wall was measured using the MC array method that the authors recently proposed [24]. The hydrophobically treated silicon parallel MCs used for this measurement had a width of 20 μm , a depth of 5 μm , and a length of 2000 μm . All of the measurements were carried out at T_C between 10 and 55°C.

The number-weighted average droplet diameter ($d_{\text{av,drop}}$) was determined based on the diameters of 200 droplets measured using WinRoof software (Mitami Co. Ltd., Fukui, Japan). CV, used as an indicator of the droplet-size distribution, was calculated by

$$\text{CV} = \frac{\sigma}{d_{\text{av,drop}}} \times 100 \quad (2)$$

where σ is the standard deviation. The droplet generation rate at an MC (f_{MC}) is given by

$$f_{MC} = \frac{1}{t}$$

(3)

where t is the droplet generation time, determined by averaging the generation time of ten consecutive droplets. The dispersed-phase velocity in an MC ($U_{d,MC}$), which influences the flow state of the dispersed phase during droplet generation, was estimated by

$$U_{d,MC} = \frac{(\pi d_{drop}^3) f_{MC}}{6 A_{MC}}$$

(4)

where A_{MC} is the MC cross-sectional area, and d_{drop} is the droplet diameter, determined by averaging the diameter of twenty droplets.

3. Results and Discussion

3.1 Physical and physicochemical properties of the liquid phases

The viscosity of the liquid phases at different temperatures is presented in Fig. 2a. The continuous-phase viscosity (η_c) and dispersed-phase viscosity (η_d) decreased as T_C increased in the range of 10°C to 55°C. Such a change in η_c and η_d is reasonable, since increasing the liquid temperature reduces the cohesive forces and increases the rate of molecular interchange [25]. The η_c and η_d data fitted well with the following exponential equations.

$$\eta_c = 1.0 \exp(-0.014T_c) \quad (5)$$

$$\eta_d = 9.0 \exp(-0.031T_c) \quad (6).$$

The viscosity ratio (ξ), defined as η_d/η_c , decreased with increasing T_C from 7.5 to 3.4 (Fig. 2a). The ξ data also had a high correlation (coefficient of determination (R^2): 0.99) with the exponential equation.

$$\xi = \eta_d/\eta_c = 8.8 \exp(-0.017T_c) \quad (7).$$

Figure 2b illustrates the influence of temperature on the equilibrium interfacial tension. The equilibrium interfacial tension of the W/O system in the presence of CR-310 ($\gamma_{eq,E}$) used for the MCE experiments decreased exponentially by 1.5 times as T_C increased from 10 to 55°C, fitting well with the following equation.

$$\gamma_{eq,E} = 4.6 \exp(-0.009T_C) \quad (8).$$

This decrease in $\gamma_{eq,E}$ was observed for the soybean oil-in-Milli-Q water containing a nonionic hydrophilic surfactant system [24]. The equilibrium interfacial tension of the W/O system in the absence of CR-310 ($\gamma_{eq,NE}$) also decreased exponentially with increasing T_C by 1.2 times. The equation that correlates with the plots is

$$\gamma_{eq,NE} = 34.2 \exp(-0.005T_C). \quad (9).$$

At each temperature, the addition of CR310 led to a considerable decrease in $\gamma_{eq,NE}$ by 7.7 to 9.1 times.

The contact angle data obtained by the MC array method are presented in Fig. 3. The contact angle of the dispersed phase (θ_d) to the hydrophobically modified MC wall increased with increasing T_C . This increase in θ_d is assumed to be related to the rise in the solubility of water in the continuous phase as a function of T_C [26, 27]. The θ_d data fitted the following linear equation well.

$$\theta_d = 0.26T_C + 150 \quad (10).$$

This result is opposite to the change in θ_d to the hydrophilic MC wall [22]. Previous studies considered soybean oil as the dispersed phase and the Milli-Q water containing a surfactant as the continuous phase. The micrographs and θ_d values in Fig. 3 demonstrate that the MC wall was preferentially wetted by the continuous phase and was not wetted by the dispersed phase. In addition, the θ_d values suggest that monodisperse W/O emulsions are stably produced using the W/O system described in Section 2.3 and the hydrophobic MC array chip used in this study [16].

3.2 Droplet generation characteristics

A gradual increase in ΔP_d caused the dispersed phase to enter the terrace in front of the MC inlets. When ΔP_d reached the breakthrough pressure ($\Delta P_{d,bt}$), the dispersed phase started to pass through the MCs, leading to the periodic generation of aqueous droplets (Fig. 4a). $\Delta P_{d,bt}$ must be understood for performing successful MCE. $\Delta P_{d,bt}$ obtained from the experiments decreased as T_C increased from 10 to 55°C (Fig. 4b), which is analogous to the variation in $\gamma_{eq,E}$ (Fig. 2b). $\Delta P_{d,bt}$ values were estimated by the following equation based on the capillary pressure equation [30]:

$$\Delta P_{d,bt} = \frac{4\gamma_{eq,E}|\cos\theta_d|}{d_{MC}} \quad (11)$$

where d_{MC} is the MC hydraulic diameter. The theoretical $\Delta P_{d,bt}$ data obtained using Eq. (11) are plotted in Fig. 4b. The temperature dependence of the theoretical $\Delta P_{d,bt}$ was similar to that of the experiment $\Delta P_{d,bt}$, whereas the theoretical $\Delta P_{d,bt}$ was lower than the experiment $\Delta P_{d,bt}$ by ~55% at each T_C . This difference in $\Delta P_{d,bt}$ may be attributable to the hydrodynamic resistance of the advancing dispersed phase on the chip.

Figure 5 presents screen shots of droplet generation from a channel at a $\Delta P_{d,bt}$ of 1.2 kPa (T_C : 55°C). The water-oil interface stabilized by hydrophobic surfactant molecules moved smoothly on the terrace and in the well, and the interfacial shape was symmetric to the center line of each MC during the entire droplet generation process. This result indicates that attractive force did not act between the non-charged chip surface and the dispersed phase stabilized by nonionic CR-310. Successful droplet generation is reasonable because of the high θ_d value of >150°. Uniform aqueous droplets were periodically generated from the MCs at $\Delta P_{d,bt}$, irrespective of T_C (Fig. 4a). Figure 6 illustrates the influence of temperature on $d_{av,drop}$ and CV of the produced W/O emulsions. $d_{av,drop}$ depended slightly on T_C and ranged between 18 and 20 μm . The temperature dependence on $d_{av,drop}$ obtained from this study was similar to

that on the $d_{av,drop}$ of the O/W emulsions produced by MCE in our previous publications [22,24]. All of the resultant W/O emulsions had a CV of less than 5%, demonstrating that monodisperse W/O emulsions are produced by MCE over a wide temperature range. The results in Fig. 6 also suggest the possibility of tuning the size of aqueous droplets.

Figures 7 to 9 present the first results that quantitatively demonstrate the influence of $U_{d,MC}$ on the generation of W/O emulsion droplets by MCE. Figures 7a and 8 show the influence of $U_{d,MC}$ on $d_{av,drop}$ and detachment time (t_{det}) at different temperatures. t_{det} is defined as follows [17]. The detachment process starts when the tip of the dispersed phase expanding on the terrace reaches the terrace outlet (Fig. 5c). The end point of the detachment process is the moment when pinch-off of the neck on the terrace is completed (Fig. 5e) and a droplet is generated. t_{det} is the period between the preceding start and end points. Below a critical $U_{d,MC}$, $d_{av,drop}$ was not influenced by $U_{d,MC}$ (Fig. 7a), and uniform droplets were generated from the MCs (Fig. 7b). t_{det} was inversely proportional to $U_{d,MC}$ in this case (Fig. 8), indicating that $U_{d,MC}$ does not influence the volume of the dispersed phase that expands in the well during the detachment process. Above the critical $U_{d,MC}$, $d_{av,drop}$ steeply increased with increasing $U_{d,MC}$ (Fig. 7a), and non-uniform, larger droplets were generated from the MCs (Fig. 7c). t_{det} also increased with increasing $U_{d,MC}$ above the critical value, confirming the steep increase in $d_{av,drop}$. The droplet size trends in Fig. 7a are probably appropriate, since similar trends have been reported for the generation of O/W emulsion droplets by MCE [22,24,29]. The critical $U_{d,MC}$ increased gradually as T_C increased (Fig. 7a), and the critical $U_{d,MC}$ at 55°C was 2.9 times higher than that at 10°C. Figure 9a illustrates the influence of $U_{d,MC}$ on f_{MC} at different temperatures. At each T_C , f_{MC} increased linearly with increasing $U_{d,MC}$ below a critical value, and the maximum f_{MC} was observed near the critical $U_{d,MC}$. f_{MC} above the critical $U_{d,MC}$ was much smaller than the maximum f_{MC} , due to the prolonged process of detachment from the terrace outlet. As can be seen in Fig. 9b, the maximum f_{MC} increased exponentially with increasing T_C . The fitted exponential equation with R^2 of 0.99 is

$$f_{MC,max} = 8.5 \exp(0.0032T_c) \quad (12)$$

where $f_{MC,max}$ is the maximum droplet generation rate for an MC. The increase in $f_{MC,max}$ is primarily attributable to the considerable decrease in viscosity of the two phases, since their viscosity greatly influences the movement of the water-oil interface on the terrace and in the well during droplet generation. The result in Fig. 9b also demonstrates that droplet productivity could be improved by performing MCE at a high T_C . It should be noted that the operating temperature must be controlled by appropriately considering the properties of all of the emulsion components.

3.3 Analysis of flow of the dispersed phase during droplet generation using dimensionless numbers

In MC emulsification, the flow of the dispersed phase during droplet generation is dominated by the balance between the interfacial tension force and the viscous force, expressed as the capillary number of the dispersed phase (Ca_d) [30]. We recently proposed an adapted capillary number that considers the influence of the wettability of the dispersed phase to the MC array surfaces, as a large portion of the water-oil interface on the terrace attaches to its walls during the detachment process [22]. This adapted capillary number ($Ca_{d,E}^\theta$) is defined as

$$Ca_{d,E}^\theta = \frac{\eta_d U_{d,MC}}{\gamma_{eq,E} |\cos \theta_d|} \quad (13)$$

Figure 10a illustrates the influence of $Ca_{d,E}^\theta$ on the dimensionless droplet diameter (\bar{d}), defined as

$$\bar{d} = \frac{d_{drop}}{h_{terrace}} \quad (14)$$

where h_{terrace} is the terrace height. The trends in \bar{d} changed remarkably near the critical $Ca_{d,E}^{\theta}$ designated in Fig. 10a, irrespective of T_c . \bar{d} remained almost constant at about 4 below the critical $Ca_{d,E}^{\theta}$, and the interfacial tension force dominated successful droplet generation in this region. By contrast, \bar{d} was greatly sensitive to $Ca_{d,E}^{\theta}$ above the critical value, as the viscous force effective in this region elongated the detachment process. The critical $Ca_{d,E}^{\theta}$ was temperature-dependent, and the maximum/minimum critical $Ca_{d,E}^{\theta}$ ratio was 1.9. During the rapid detachment process, the critical detachment time decreased from 0.08 to 0.02 s at T_C between 10 to 55°C. For soybean oil-in-water emulsions containing 1% SDS, the critical detachment time decreased from 0.15 to 0.02 s at T_C from 10 to 70°C [22]. These results indicate that the surfactant molecules may adsorb little to a newly created water-oil interface, and that the interfacial tension in the absence of surfactant ($\gamma_{\text{eq,NE}}$) has to be included in the adapted capillary number as follows.

$$Ca_{d,NE}^{\theta} = \frac{\eta_d U_{d,MC}}{\gamma_{\text{eq,NE}} |\cos \theta_d|} \quad (15)$$

As depicted in Fig. 10b, the range of the critical $Ca_{d,NE}^{\theta}$ becomes narrower, with a maximum/minimum ratio of 1.2. This result demonstrates that $Ca_{d,NE}^{\theta}$ as proposed here is a useful indicator for understanding the flow transition of the dispersed phase during droplet generation.

4. Conclusions

Our results have demonstrated that MCE using a hydrophobic MC array chip is capable of producing monodisperse W/O emulsions with CV below 5% over a wide T_C range (10°C to 55°C). The contact angle data strongly suggested the stable generation of uniform aqueous droplets via MC arrays at T_C applied in this study. The resultant droplet size depended slightly on the operating temperature, indicating the possibility of finely tuning the droplet size by

temperature. At each T_C , the size of the generated aqueous droplets was almost independent of $U_{d,MC}$ below a critical value, which is the first quantitative finding reporting the influence of $U_{d,MC}$ on the size of W/O emulsion droplets. By contrast, their size was highly sensitive to $U_{d,MC}$ above the critical value. High-temperature MC emulsification is useful for increasing the productivity of uniform aqueous droplets if the emulsion components are insensitive to heating. An adapted capillary number that considers the influences of the wettability and dynamic surfactant adsorption was demonstrated to be a useful indicator for understanding the flow transition of the dispersed phase during droplet generation.

Acknowledgement

This work was supported by the Food Nanotechnology Project of the Ministry of Agriculture, Forestry, and Fisheries of Japan.

Nomenclature

A_{MC}	channel cross-sectional area [m^2]
$Ca_{d,E}^0$	adapted capillary number of a dispersed phase in the presence of surfactant
	[–]
$Ca_{d,NE}^0$	adapted capillary number of a dispersed phase in the absence of surfactant
	[–]
CV	coefficient of variation [–]
d_{drop}	droplet diameter [m]
\bar{d}	dimensionless droplet diameter [–]
$d_{av,drop}$	number-weighted mean droplet diameter [m]
d_{MC}	channel hydraulic diameter [m]
f_{MC}	droplet generation rate per channel [s^{-1}]
$f_{MC,max}$	maximum droplet generation rate per channel [s^{-1}]

380	g	acceleration due to gravity [m s^{-2}]
381	Δh_d	height of a dispersed-phase chamber [m]
382	h_{terrace}	terrace height [m]
383	ΔP_d	pressure applied to a dispersed phase [Pa]
384	$\Delta P_{d,\text{bt}}$	breakthrough pressure of a dispersed phase [Pa]
385	T_C	Celsius temperature [$^{\circ}\text{C}$]
386	t_{det}	detachment time [s]
387	t	droplet generation time [s]
388	$U_{d,\text{MC}}$	flow velocity of a dispersed phase inside a channel [m]
389		
390	<i>Greek symbols</i>	
391	$\gamma_{\text{eq,E}}$	equilibrium interfacial tension in the presence of surfactant [N m^{-1}]
392	$\gamma_{\text{eq,NE}}$	equilibrium interfacial tension in the absence of surfactant [N m^{-1}]
393	η_c	viscosity of a continuous phase [Pa s]
394	η_d	viscosity of a dispersed phase [Pa s]
395	θ_d	contact angle of a dispersed phase [deg]
396	ξ	viscosity ratio of a dispersed phase to a continuous phase [–]
397	ρ_d	density of a dispersed phase [kg m^{-3}]
398	σ	standard deviation [m]
399		

References

- [1] S. van der Graaf, C.Y.P.H. Schroën, R.M. Boom, Preparation of double emulsions by membrane emulsification-a review. *J. Membr. Sci.* 251 (2005) 7.
- [2] J. Surh, G.T. Vladislavljević, S. Mun, D.J. McClements, Preparation and characterization of water/oil and water/oil/water emulsions containing biopolymer-gelled water droplets. *J. Agric. Food Chem.* 55 (2007) 175.
- [3] I. Kobayashi, S. Ichikawa, M.A. Neves, T. Kuroiwa, M. Nakajima, Formulation of lipid micro/nanodispersions systems, in: M. Ahmad (Ed.), *Lipids in Nanotechnology*, AOCS Press, Urbana, 2011, pp. 95-134.
- [4] T. Nakashima, M. Shimizu, M. Kukizaki, Particle control of emulsions by membrane emulsification and its applications. *Adv. Drug Deliv. Rev.* 45 (2000) 47.
- [5] D.J. McClements, *Food emulsions: Principles, practice, and techniques* (2nd Ed.), CRC Press, Boca Raton, 2004, pp. 9-17.
- [6] C. Orr, Emulsion droplet size, in: P. Becher (Ed.), *Encyclopedia of emulsion technology*, vol. 1, Marcel Dekker, New York, 1983, pp. 369-404.
- [7] M. Saito, L.J. Yin, KobayashiI, M. Nakajima, Comparison of stability of bovine serum albumin-stabilized emulsions prepared by microchannel emulsification and homogenization. *Food Hydrocoll.* 20 (2005) 1020.
- [8] T.G. Mason, A.H. Krall, H. Gang, J. Bibette, D.A. Weitz, Monodisperse emulsions properties and uses in: P. Becher, *Encyclopedia of Emulsion Technology*, vol. 2, Marcel Dekker, New York, 1996, pp. 299-335.
- [9] M. Kukizaki, M. Goto, Preparation and evaluation of uniformly sized solid lipid microcapsules using membrane emulsification. *Colloids Surf. A* 293 (2006) 94.
- [10] T. Nakashima, M. Shimizu and M. Kukizaki, Membrane emulsification by microporous glass. *Key Eng. Mater.* 61/62 (1991) 513.

- [11] U. Lambrich, H. Schubert, Emulsification using microporous systems. *J. Membr. Sci.* 257 (2005) 76.
- [12] M. Kukizaki, Relation between salt rejection and electrokinetic properties on Shirasu porous glass (SPG) membranes with nano-order uniform pores. *Sep. Purif. Technol.* 69 (2009) 87.
- [13] C.J. Cheng, L.Y. Chu, R. Xie, Preparation of highly monodisperse W/O emulsions with hydrophobically modified SPG membranes. *J. Colloid Interface Sci.* 300 (2006) 375.
- [14] C.J. Cheng, L.Y. Chu, J. Zhang, M.Y. Zhou, F. Xie, Preparation of monodisperse poly(N-isopropylacrylamide) microspheres and microcapsules via Shirasu-porus-glass membrane emulsification. *Desalination* 234 (2008) 184.
- [15] T. Kawakatsu, Y. Kikuchi, M. Nakajima, Regular sized cell creation in microchannel emulsification by visual microprocessing method. *J. Am. Oil Chem. Soc.* 74 (1997) 317.
- [16] T. Kawakatsu, G. Trägårdh, Ch. Trägårdh, Production of W/O/W emulsions and S/O/W pectin microcapsules by microchannel emulsification. *Colloids Surf. A* 189 (2001) 257.
- [17] S. Sugiura, M. Nakajima, H. Ushijima, K. Yamamoto, M. Seki, Preparation characteristics of monodispersed water-in-oil emulsions using microchannel emulsification. *J. Chem. Eng. Japan* 34 (2001) 757.
- [18] I. Kobayashi, H. Sayumi, K. Takamori, Y. Zhang, K. Uemura, M. Nakajima, High-aspect-ratio through-hole array microfabricated in a PMMA plate for monodisperse emulsion production. *Microsist. Technol.* 14 (2008) 1349.
- [19] I. Kobayashi, Y. Murayama, T. Kuroiwa, K. Uemura, M. Nakajima, Production of monodisperse water-in-oil emulsions consisting of highly uniform droplets using asymmetric straight-through microchannel arrays. *Microfluid. Nanofluid.* 7 (2009) 107.
- [20] H. Liu, M. Nakajima, T. Kimura, Production of Monodispersed Water-in-Oil Emulsions Using Polymer Microchannels. *J. Am. Oil Chem. Soc.* 81 (2004) 705.

- [21] S. Iwamoto, K. Nakagawa, S. Sugiura, M. Nakajima, Preparation of gelatin microbeads with a narrow size distribution using microchannel emulsification. *AAPS Pharm. Sci. Tech.* 3 (2002) 25.
- [22] K. Butron Fujiu, I. Kobayashi, K. Uemura, M. Nakajima, Temperature effect on microchannel oil-in-water emulsions. *Microfluid. Nanofluid.* 10 (2011) 773.
- [23] S. Sugiura, T. Kuroiwa, M. Kagota, M. Nakajima, S. Sato, S. Mutakata, P. Walde, S. Ichikawa, Novel method for obtaining homogeneous giant vesicles from a monodisperse water-in-oil emulsion prepared with a microfluidic device. *Langmuir* 24 (2008) 4581.
- [24] K. Butron Fujiu, I. Kobayashi, M.A. Neves, K. Uemura, M. Nakajima, Effect of temperature on production of soybean oil-in-water emulsions by microchannel emulsification using different emulsifiers. *Food Sci. Technol. Res.* 17 (2011) 77.
- [25] E. Poling, J.M. Prausnitz, J.P. O'Connell, The properties of gases and liquids. 5th Edition, Chapter 9, Viscosity, McGraw-Hill, New York, 2001, pp. 9.51-9.54.
- [26] V.G. Skripka, Solubility of water in normal alkanes at elevated temperatures and pressures. *Chem Tech Fuel Oil* 15 (1979) 88.
- [27] A. Mączyński, M. Góral, G.B. Wiśmiewska, A. Skrzecz, D. Shaw, Mutual solubilities of water and alkanes. *Monatshefte für Chemie* 134 (2003) 333.
- [28] Carey A. Francis, *Organic Chemistry* (4th Ed.), McGraw-Hill, 2000, pp. 71-74.
- [29] J. Tong, M. Nakajima, H. Nabetani, Y. Kikuchi, Surfactant effect on production of monodispersed microspheres by microchannel method emulsification. *J. Surfactants Detergents* 3 (2000) 285.
- [30] S. Sugiura, M. Nakajima, N. Kumazawa, S. Iwamoto, M. Seki, Characterization of spontaneous transformation-based droplet formation during microchannel emulsification. *J. Phys. Chem. B* 106 (2002)

Figure Captions

Fig. 1. (a) Schematic drawing of the experiment setup for MCE. (b, c) Schematic drawings of the MC array chip and part of an MC array. Dimensions of the channel and terrace are denoted as micrometers. (d) Schematic three-dimensional drawing of droplet generation via part of an MC array.

Fig. 2. (a) Variation in the viscosity of the dispersed and continuous phases and their viscosity ratio as a function of temperature. η_d is the dispersed-phase viscosity (\bullet), η_c is the continuous-phase viscosity (\blacklozenge), and ξ is the viscosity ratio, defined as η_d/η_c (\blacktriangle). (b) Variation in the equilibrium interfacial tension as a function of temperature. All of the fitted lines (Eqs. (5)-(9)) in (a) and (b) had a coefficient of determination (R^2) exceeding 0.99.

Fig. 3. (a) Variation in the contact angle of the dispersed phase to the MC wall as a function of temperature. The fitted line (Eq. (10)) had R^2 of 0.98. (b) Optical micrographs of the water-oil interface formed in a rectangular MC at T_C of 10°C and 55°C.

Fig. 4. (a) Typical optical micrograph of the generation of W/O emulsion droplets from hydrophobic MCs. (b) Variation in breakthrough pressure as a function of temperature.

Fig. 5. A droplet generation cycle with an MC and a terrace at T_C of 55°C.

Fig. 6. Variation in the average droplet diameter and CV as functions of temperature.

Fig. 7. (a) Variation in droplet diameter at different temperatures as a function of the flow velocity of the dispersed phase. (b, c) Typical optical micrographs of droplet generation with

501 MCs at T_C of 25°C. (b) Below the critical flow velocity ($U_{d,MC} = 1.2$ mm/s). (c) Above the
502 critical flow velocity ($U_{d,MC} = 4.2$ mm/s).

503 **Fig. 8.** Variation in the detachment time at different temperatures as a function of the flow
504 velocity of the dispersed phase that flows in an MC.

505

506 **Fig. 9** (a) Variation in the droplet generation rates per MC at different temperatures as a
507 function of the flow velocity of the dispersed phase that flows in an MC. (b) Variation in the
508 maximum droplet generation rate as a function of temperature. The fitted line (Eq. (12)) had a
509 coefficient of determination (R^2) exceeding 0.99.

510

511 **Fig. 10.** (a) Variation in the dimensionless droplet diameter at different temperatures as a
512 function of the adapted capillary number of the dispersed phase ($Ca_{d,E}^\theta$) including the
513 interfacial tension in the presence of a surfactant ($\gamma_{eq,E}$). (b) Variation in the droplet diameter
514 at different temperatures as a function of the adapted capillary number ($Ca_{d,NE}^\theta$) including the
515 interfacial tension in the absence of a surfactant ($\gamma_{eq,NE}$).

516

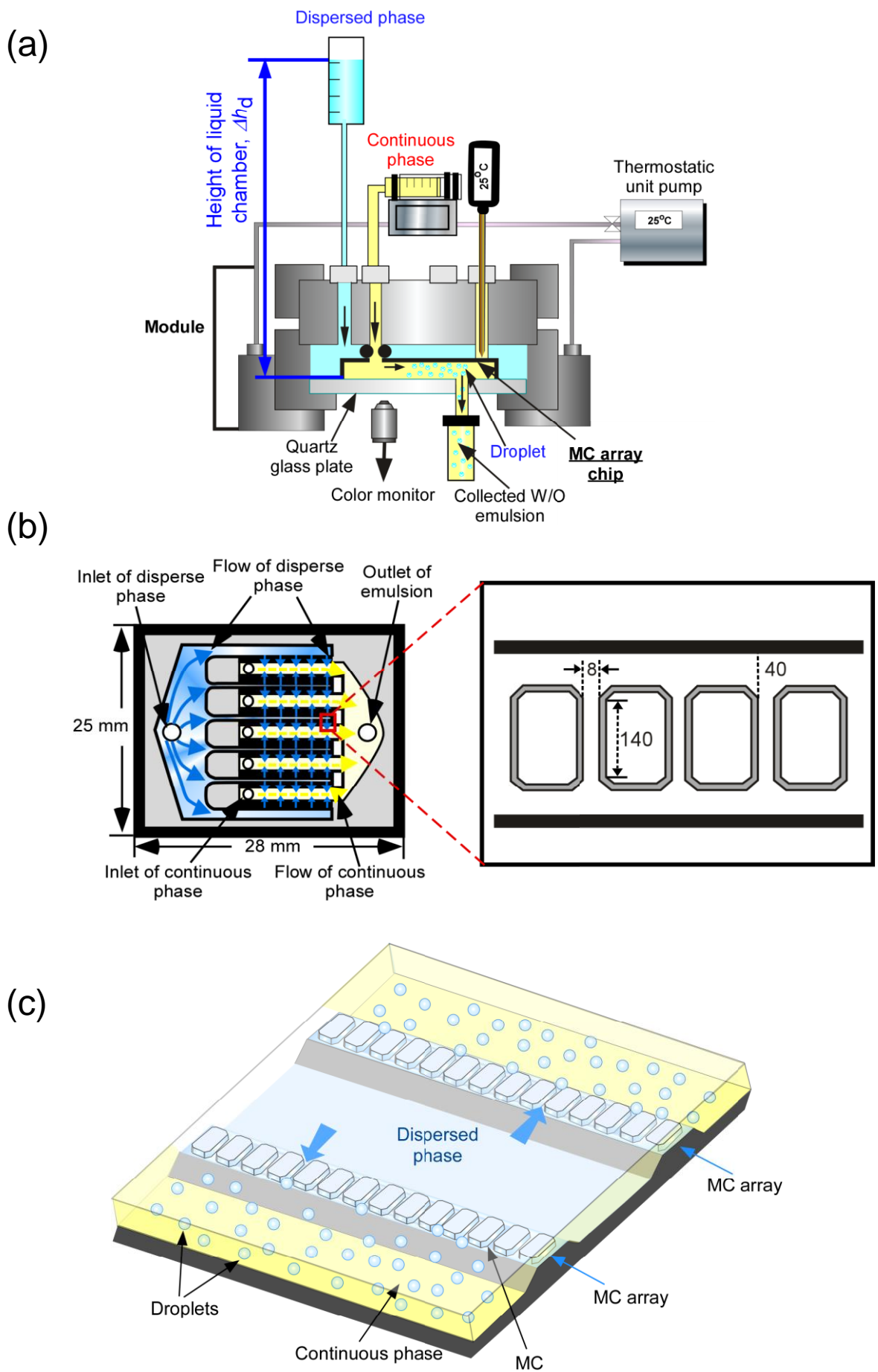


Fig. 1

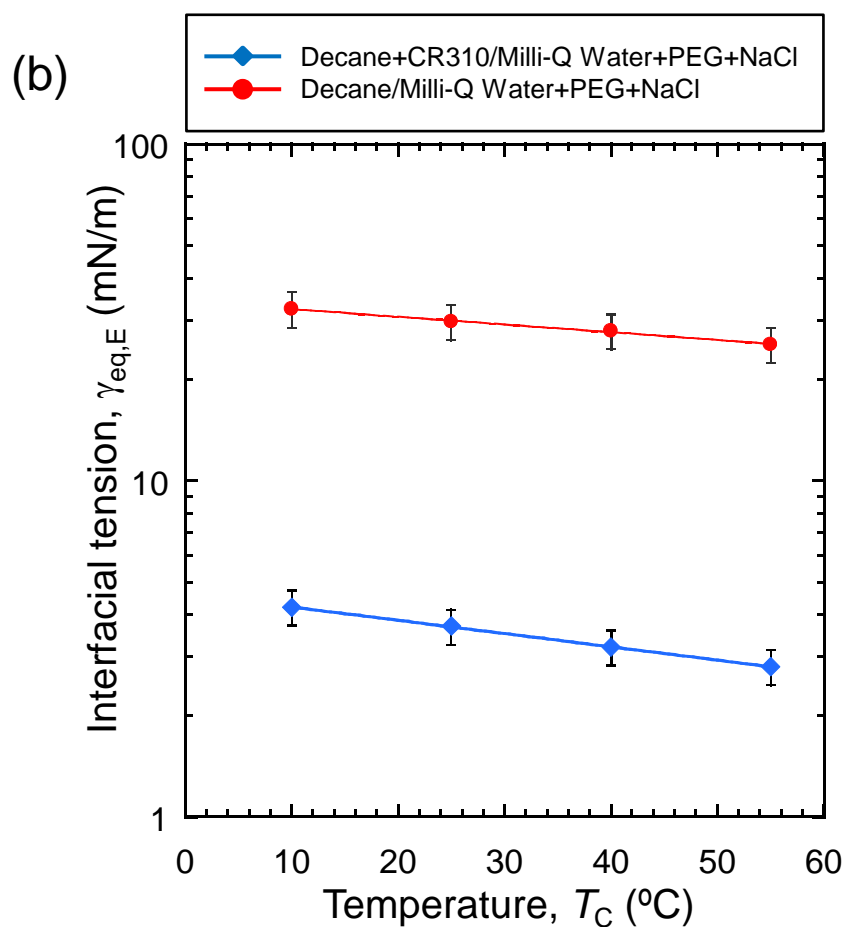
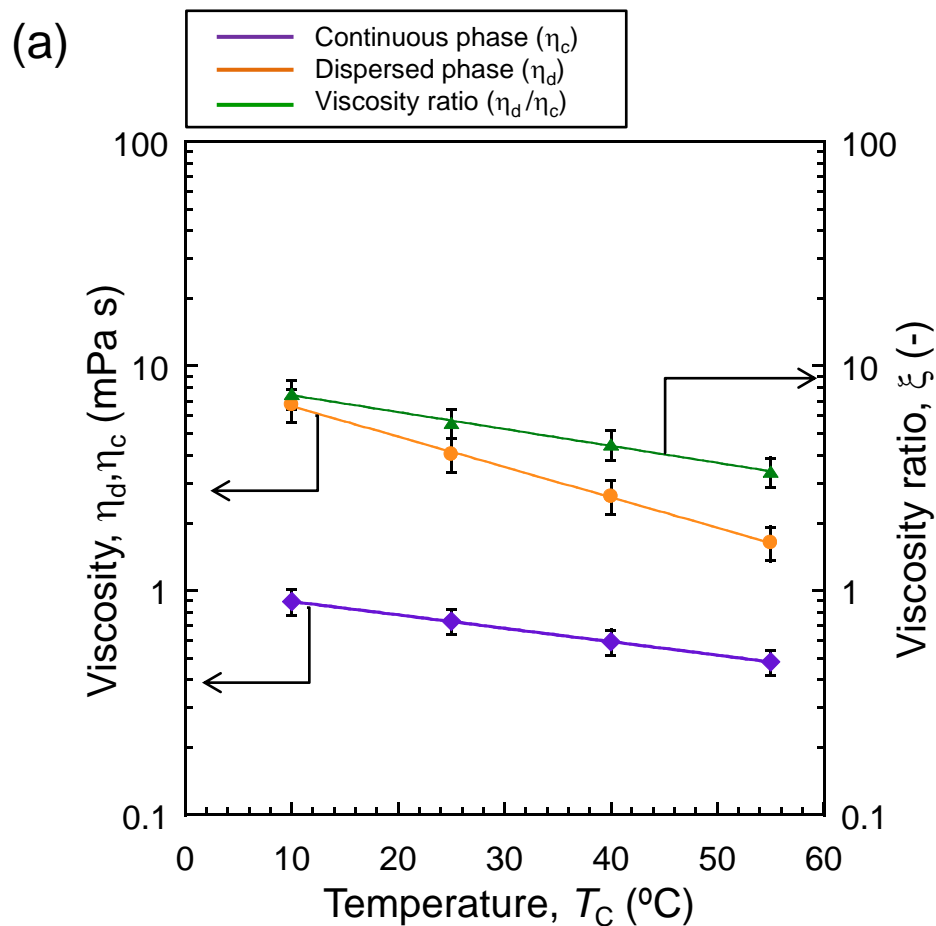


Fig. 2

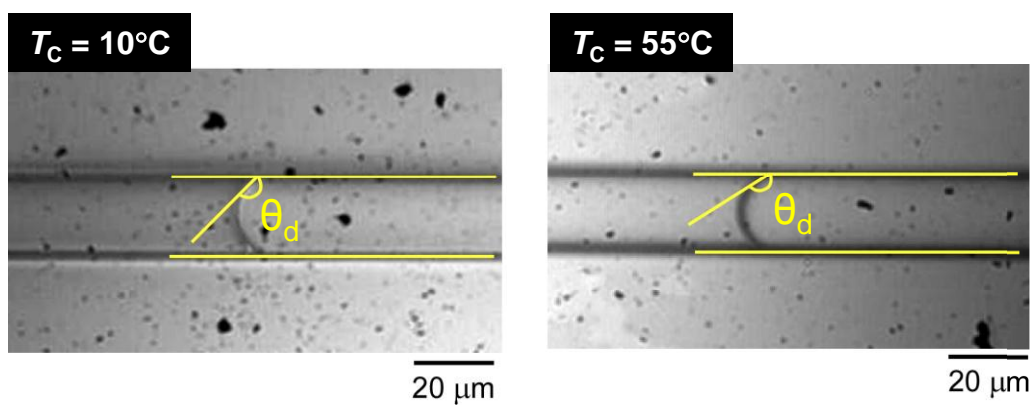
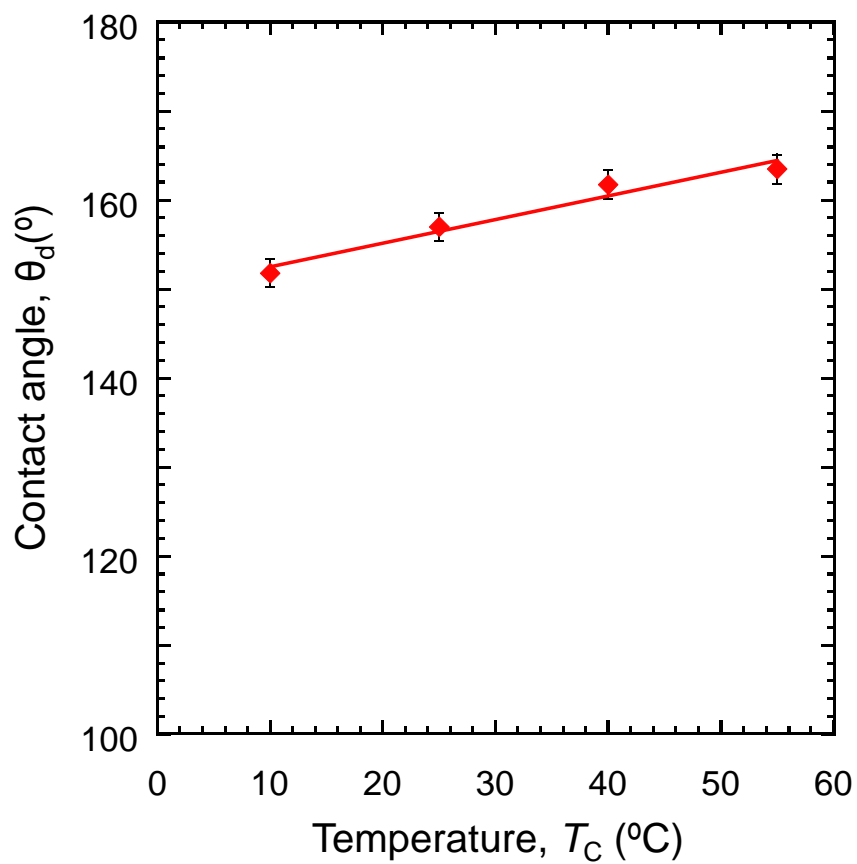


Fig. 3

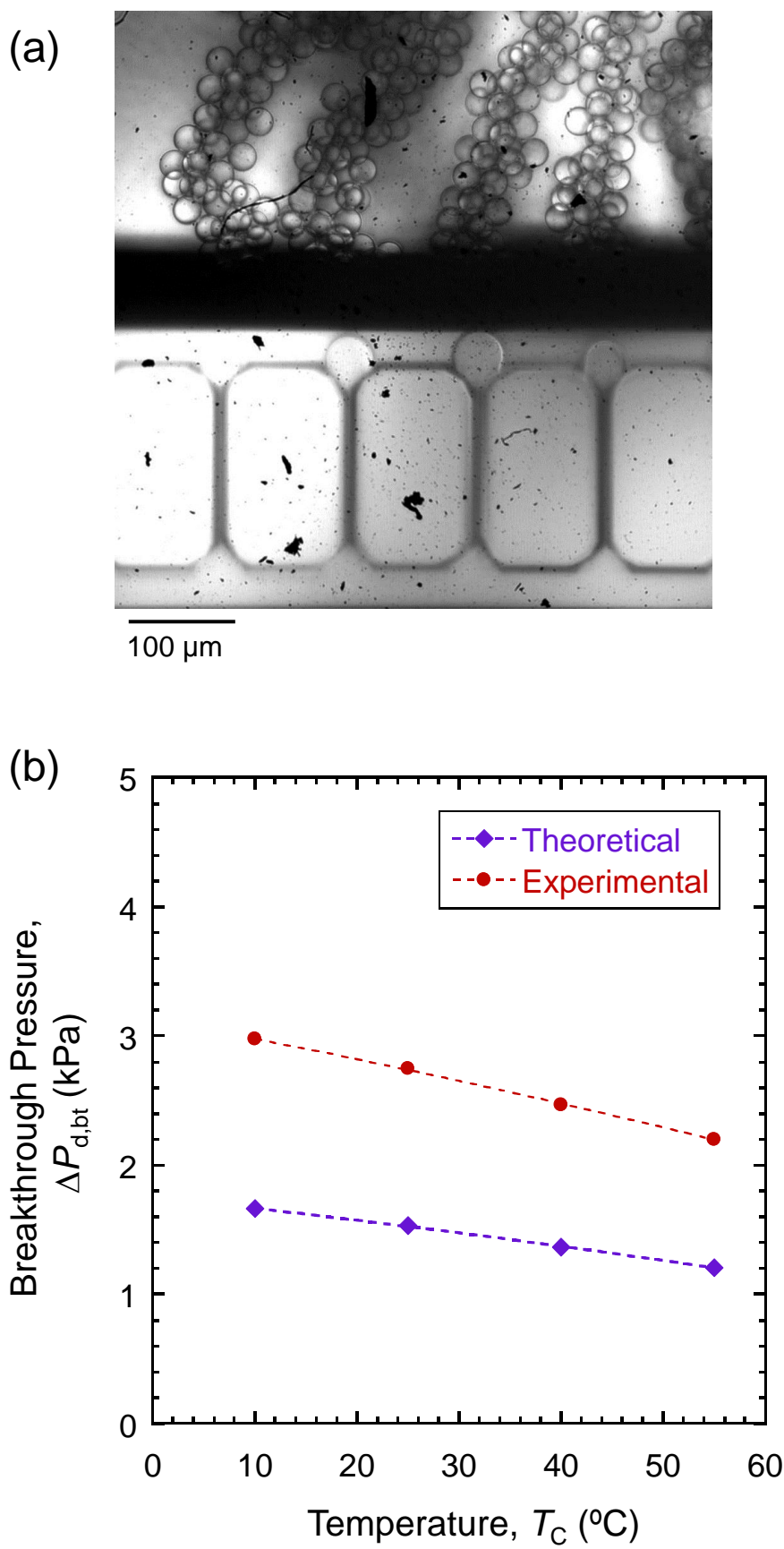


Fig. 4

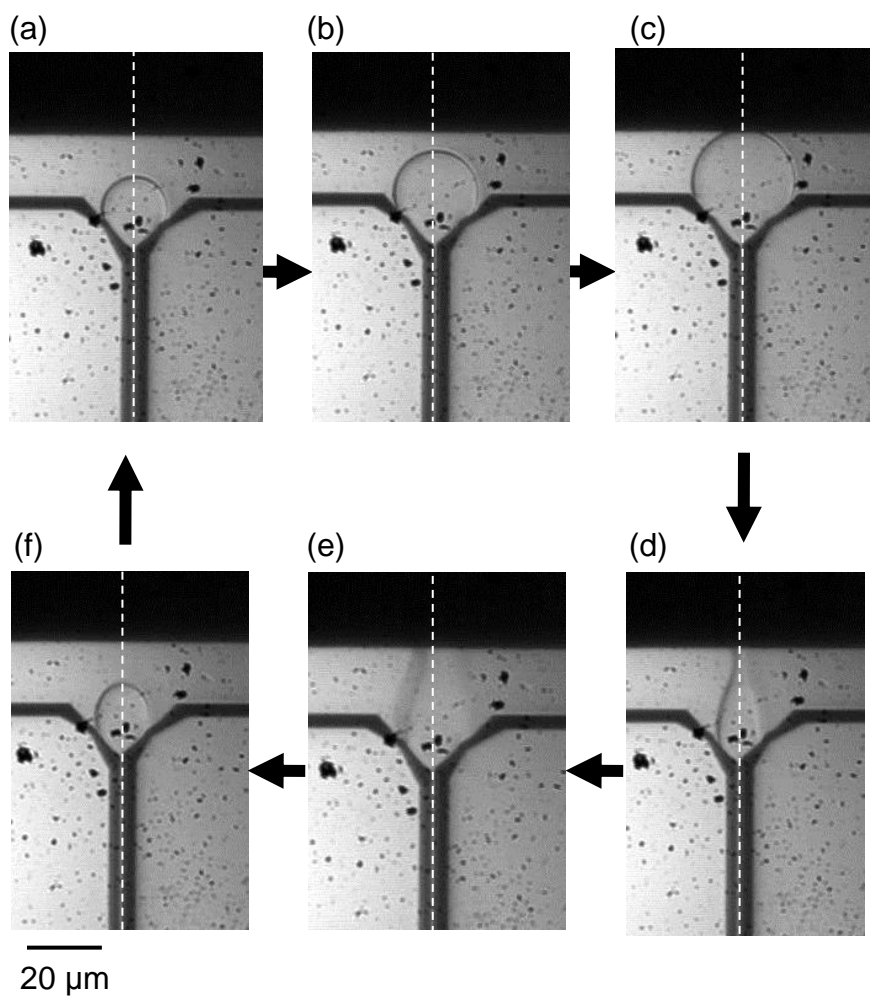


Fig. 5

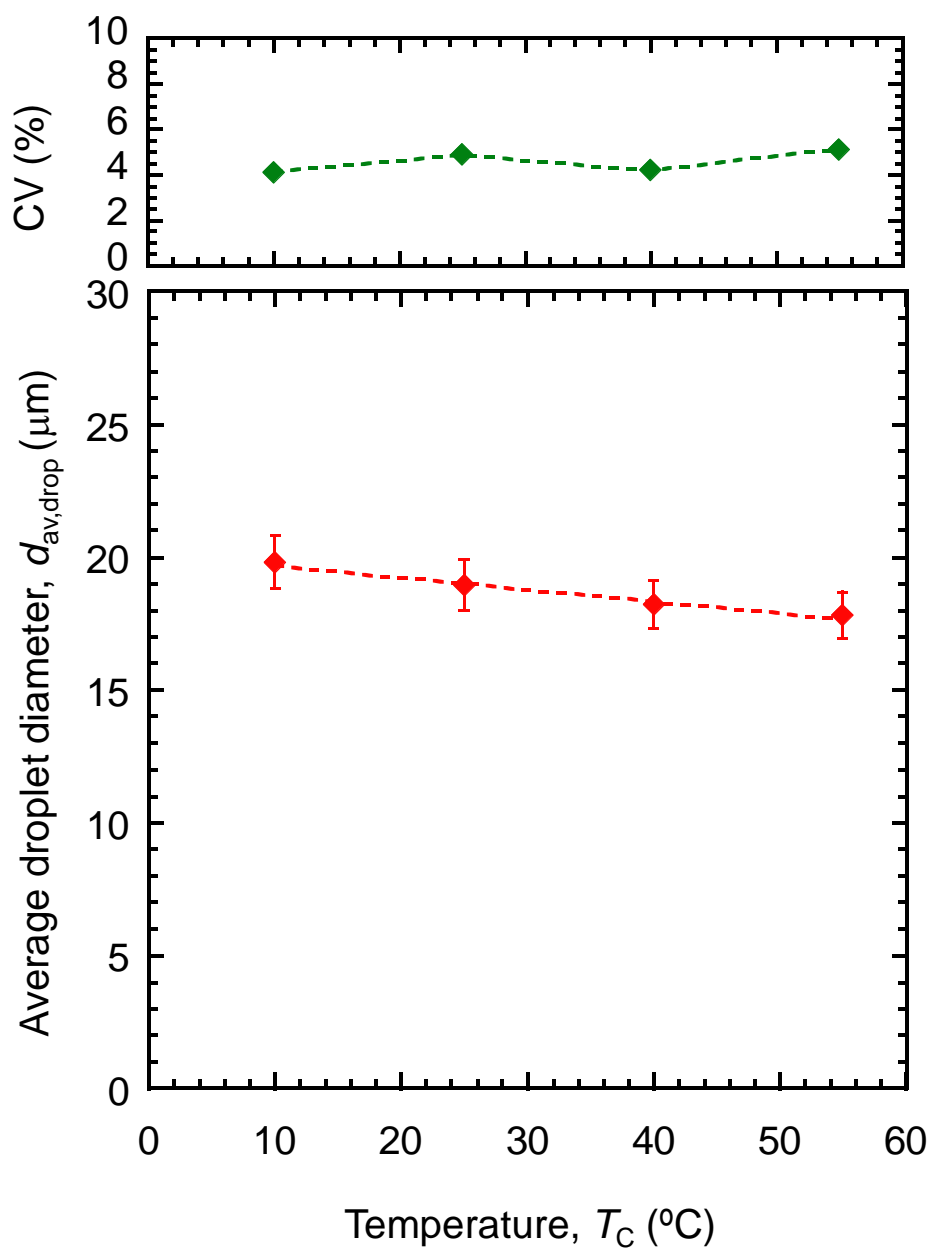


Fig. 6

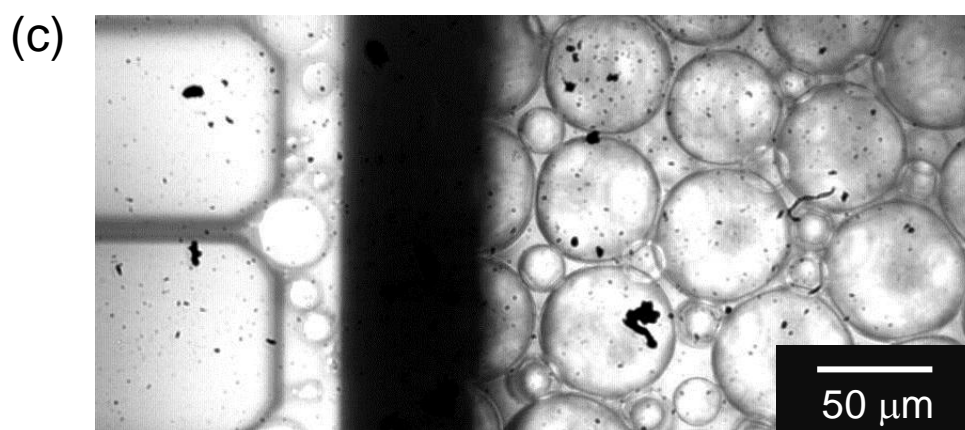
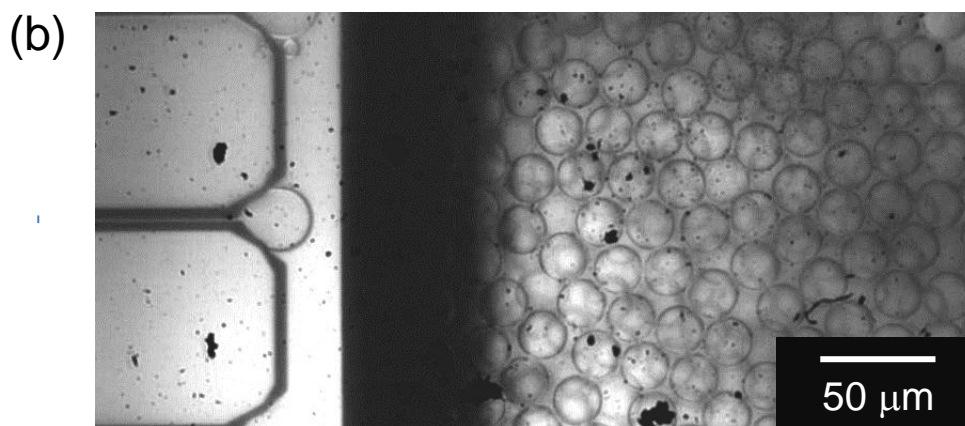
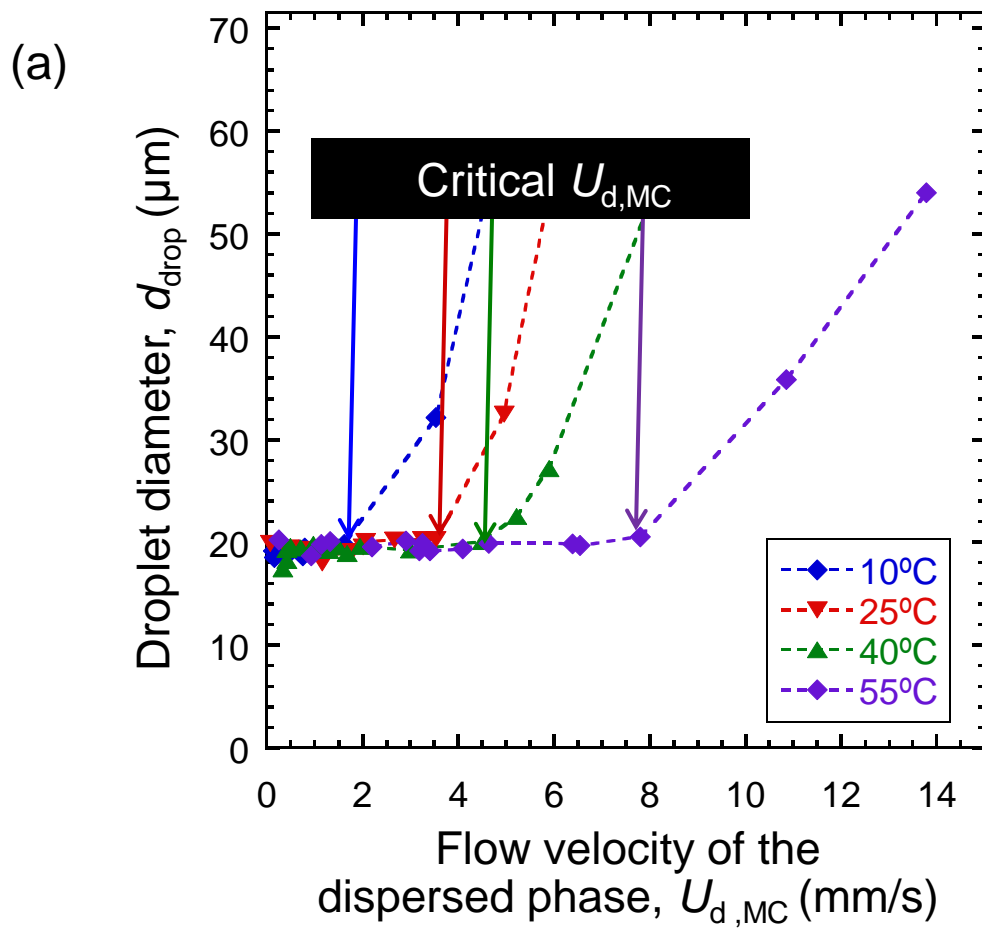


Fig. 7

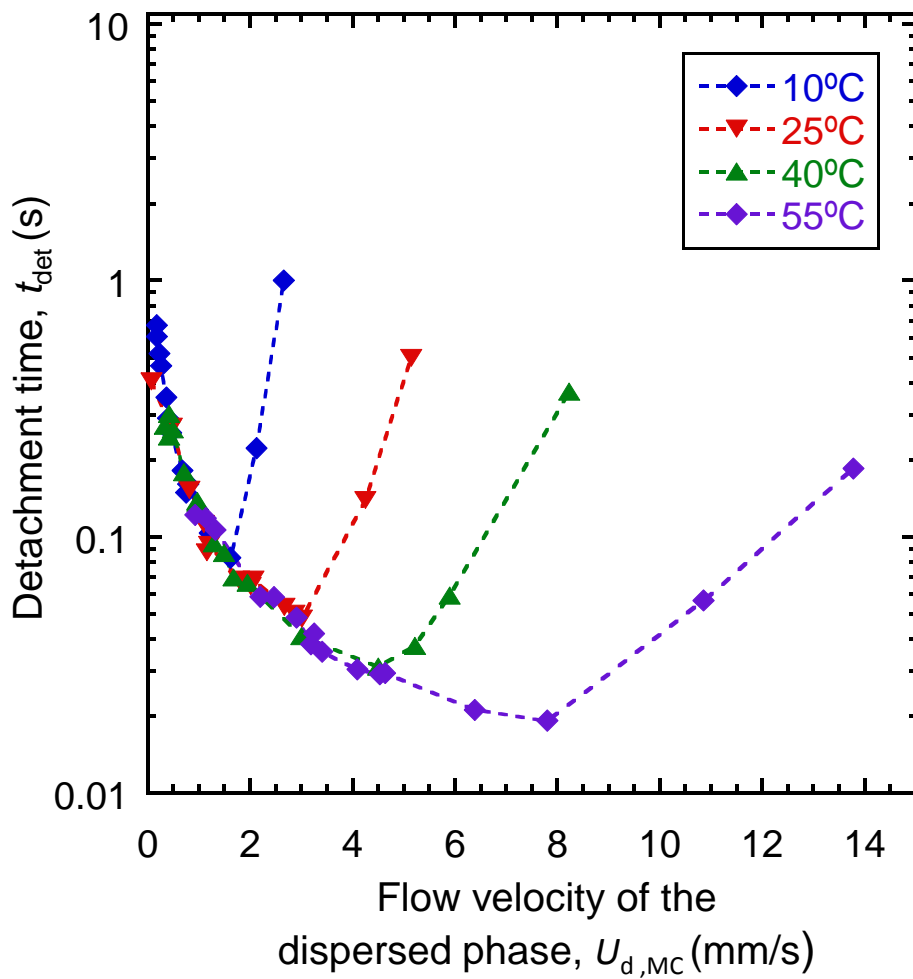


Fig. 8

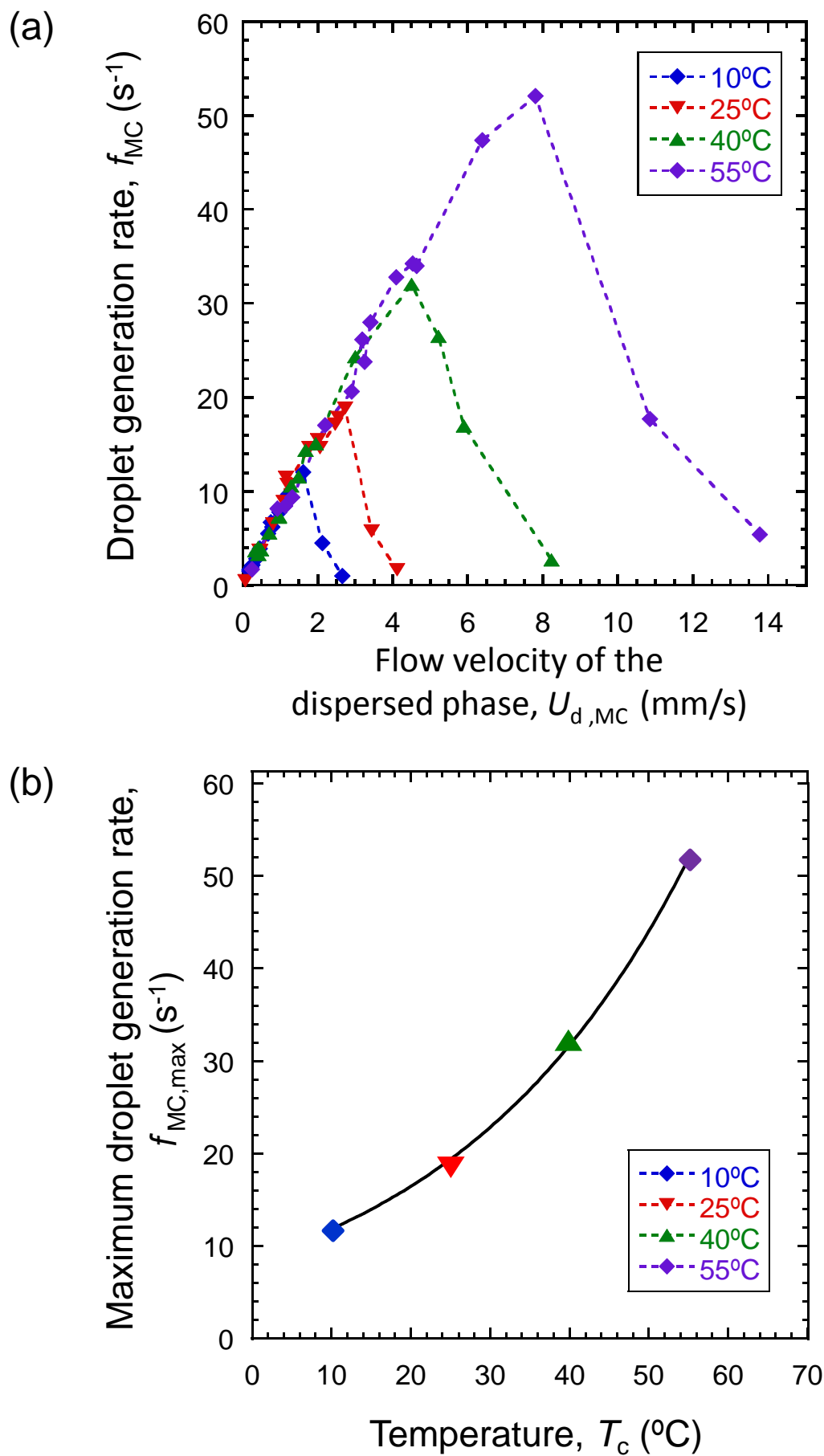


Fig. 9

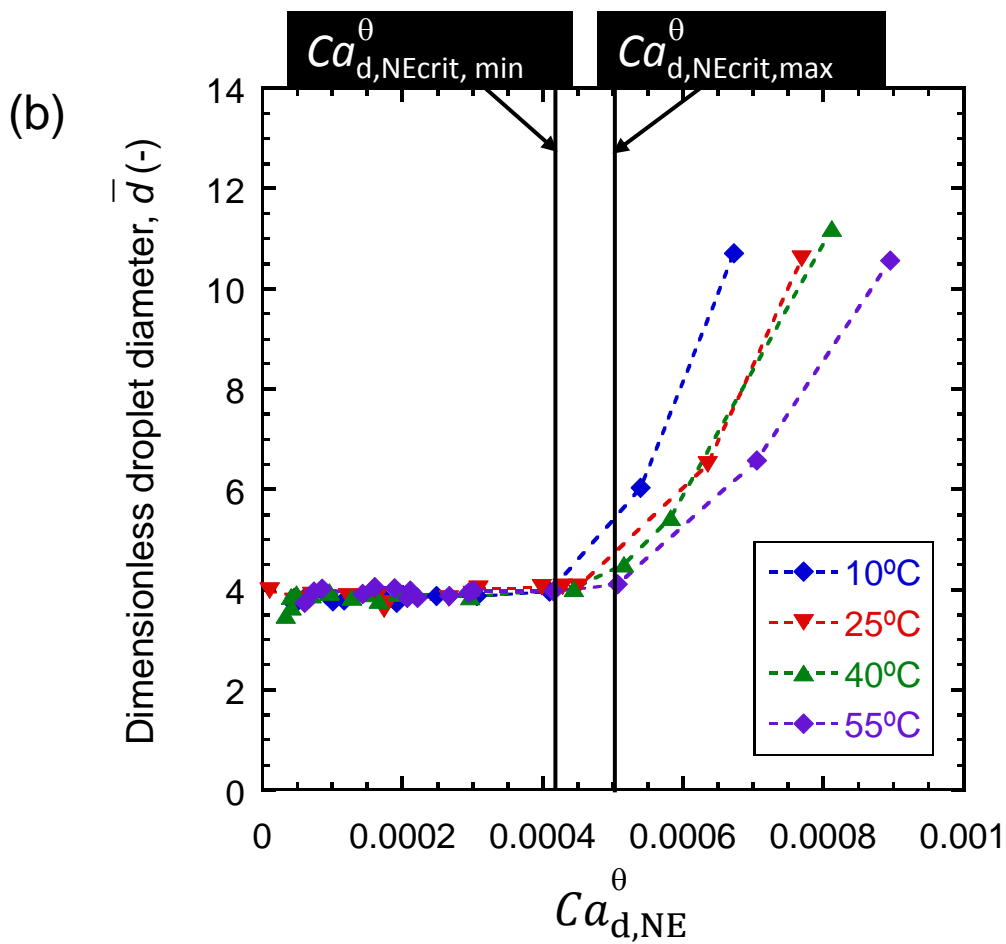
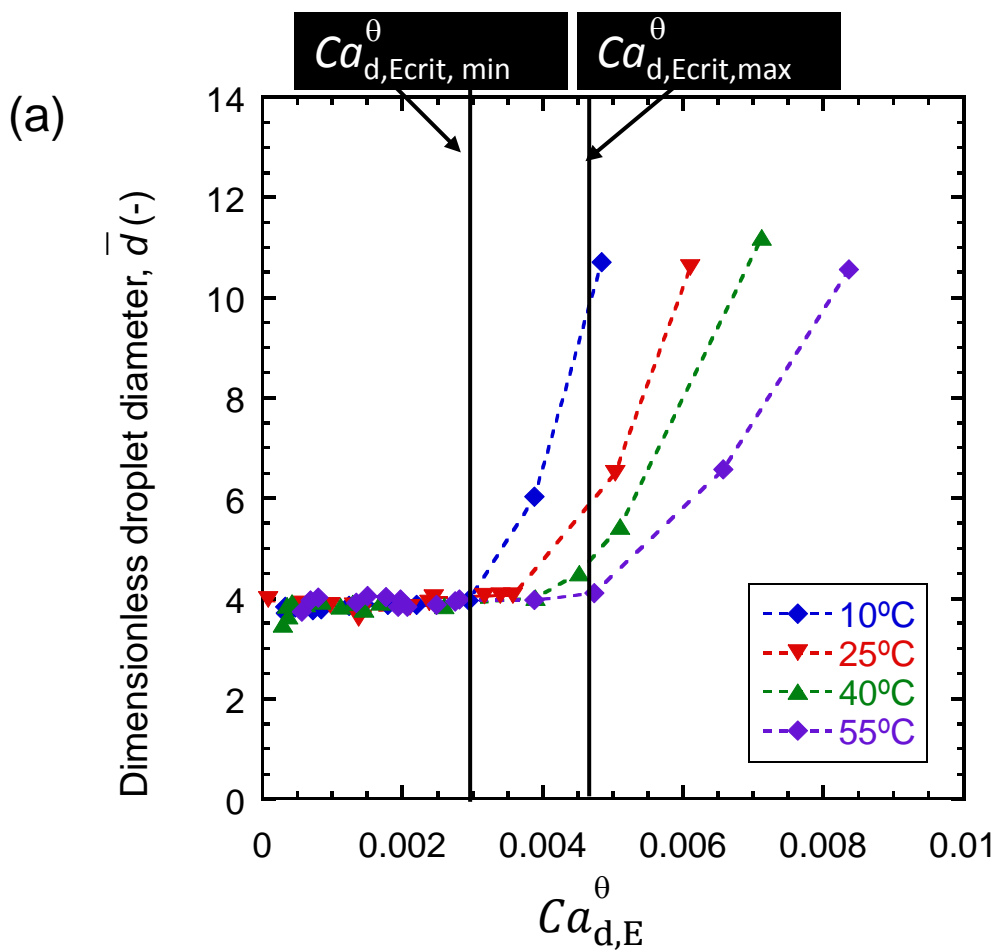


Fig. 10

Butron Fujiu *et al.*